



Compact athermalized LWIR objective lens

Hussein Mohammed Hassan² · Tawfik Abd-Elhamed Eldessouky¹ · Mohammed Medhat¹

Received: 30 January 2022 / Accepted: 30 April 2022 / Published online: 24 June 2022
© The Author(s) 2022

Abstract A new compact optical passive athermalized objective lens is designed with a focal length 120 mm and F-number 1.1. Its full field of view is 12.2° . The geometrical aberrations due to the large aperture and the wide field of view are well corrected as well as the chromatic aberration. Hence, the maximum RMS radius of the spot diagram over the full field of view is less than $17\ \mu\text{m}$ and the Strehl ratio is 0.95 at $20\ ^\circ\text{C}$. The MTF is nearly limited in diffraction over the full F.O.V. This good correction of aberrations makes the optical system gain high resolution and suitable to work with a focal plane array detector with $17\text{-}\mu\text{m}$ pixel pitch. This performance is stable over a long temperature range from $-40\ ^\circ\text{C}$ to $+65\ ^\circ\text{C}$. Moreover, the optical system is relatively compact “140 mm.” The total transmittance (after absorption consideration) of the optical system is enhanced from 6.6 to 94.07% at $\lambda = 10\ \mu\text{m}$ along the optical axis upon applying an anti-reflection coating.

Keywords Athermalization · Achromatization · IR objective lens · Infrared optical system

Introduction

Infrared imaging systems are widely used in many industrial applications, particularly in surveillance and the military. Its good response can be achieved in either total darkness, dust, smoke, light fog, rain, or snow [1–3]. In military

applications the optical system is exposed to harsh environments, so the image quality of the optical system should be maintained over the wide operating temperature range and also, the target detection with suitable resolution and long range over a wide field of view. Few materials are transparent in the infrared region rather than in the visible band, such as germanium (Ge), zinc selenide (ZnSe), zinc sulfide (ZnS), and chalcogenide glasses. In addition to the rareness of these materials, the relative changes of their refractive indices with respect to the temperature changes are very high. The temperature fluctuations lead to great changes in their indices as well as their physical parameters, such as radii and thickness. Additionally, the housing dimensions will change the separations between the optical elements. These changes lead to a focus shift, which is called thermal aberration. So the compensation of this focus shift “athermalization” and achromatization with correcting high-order aberration due to the large aperture and wide field of view for the optical system is important and challenging. There are many techniques for athermalization. The mechanical active technique requires a movement of the optical element(s), whereas the optical passive can be achieved by selecting different materials with different thermal expansions and different changes of refractive indices with temperature (dn/dT). The last one is preferred, as it is more reliable, more stable, compact, and lightweight [3–6]. However, uncooled FPA detectors have many advantages such as being lightweight, compact, low power consumption, and good reliability. Unfortunately, the sensitivity is quite small and it has a quite high noise equivalent temperature difference (NETD). To overcome these disadvantages, the F-number, which expresses the input power of the light acquired by the lens of the optical system, should be less than 2 [1, 2]. Meanwhile, the optical design by Dong Janing worked at F-number 2.2, which is not preferred for uncooled F.P.A [4]. Moreover, Jing Wang’s design has two

✉ Hussein Mohammed Hassan
Hussein.Mohammed89@yahoo.com

¹ Faculty of Science, Physics Department, Ain Shams University, Cairo, Egypt

² Arab International Optronics, Cairo, Egypt

diffractive surfaces. It will affect badly on the transmission of the optical system due to decreasing of the diffractive efficiency. This design suffers from a manufacturing difficulty for the first lens as the aspheric and diffractive are on different surfaces [5], Jiang Lun designed an objective lens with F-number 1, but the optical system designed for low Nyquist frequency “17 lp” for low detector resolution “30 μm .” This MTF performance indicates that the high-order aberrations are not well corrected [6].

Design principle

The single lens power is given by

$$\emptyset = (n - 1) \left(\frac{1}{r_1} - \frac{1}{r_2} \right) \quad (1)$$

where n is the index of refraction and r_1 and r_2 are the radii of the lens.

The change of the lens power with temperature can be derived as

$$\frac{d\emptyset}{dT} = \frac{dn}{dT} \left(\frac{1}{r_1} - \frac{1}{r_2} \right) + \left(-\frac{1}{r_1} + \frac{1}{r_2} \right) \alpha(n - 1) \quad (2)$$

where $\frac{1}{r} \frac{dr}{dT} = \alpha$ is the thermal expansion coefficient of the glass.

$$\text{hence } \frac{d\emptyset}{dT} = \left(\frac{\frac{dn}{dT}}{n - 1} - \alpha \right) \left(\frac{1}{r_1} - \frac{1}{r_2} \right) (n - 1) = \emptyset \left(\frac{\frac{dn}{dT}}{n - 1} - \alpha \right) \quad (3)$$

so that $\frac{d\emptyset}{dT} = \emptyset \beta$

$\beta = \left[\left(\frac{dn/dT}{n-1} \right) - \alpha \right]$ is the thermo-optical coefficient of the lens.

For single lens in the housing, the defocus will be

$$\frac{d\emptyset}{dT} = \emptyset (\beta - \alpha_h) \quad (4)$$

where α_h is the thermal expansion coefficient of the housing.

For an optical system consisting of many lenses (k), there are two cases.

(a) *For k lens in contact*

The total power of k elements is

$$\emptyset = \left(\frac{1}{h_1} \right) \sum_{i=1}^k h_i \emptyset_i \quad (5)$$

The achromatic condition is given by

$$\Delta f_\lambda = \left(\frac{1}{h_1 \emptyset} \right)^2 \sum_{i=1}^k h_i^2 \frac{1}{v_i} \emptyset_i = 0 \quad (6)$$

The athermalization condition is also given by

$$\Delta f_T = \left(\frac{1}{h_1 \emptyset} \right)^2 \sum_{i=1}^k h_i^2 (\beta_i \emptyset_i) + \alpha_h \emptyset = 0 \quad (7)$$

where h_i is the paraxial ray height at the i th lens and v_i is the Abbe number of the i th lens.

(b) *For k separated elements*

It can be athermalized as multiple lens groups individually, and the residual thermal aberration can be shared between these groups [7].

The power of the refractive optical element that has a diffractive surface (hybrid element) is

$$\emptyset_{\text{tot}} = \emptyset_{\text{refractive}} + \emptyset_{\text{diffractive}}$$

Material properties and material section

Table 1 shows the most commonly used materials in the infrared region with their physical properties. Germanium is the most common material used. As shown, germanium has a large Abbe number and, hence, its dispersive power is very low, so it is convenient for achieving low chromatic aberration. Additionally, it has a high refractive index, which is good for correcting spherical aberration. So germanium is a preferred material for designing optical systems in the LWIR region. Unfortunately, it has high dn/dT , which will cause high thermal aberration. With the aid of the athermal chart (Fig. 1), a good combination of materials can be used for fabricating athermalized and achromatized optical systems [8].

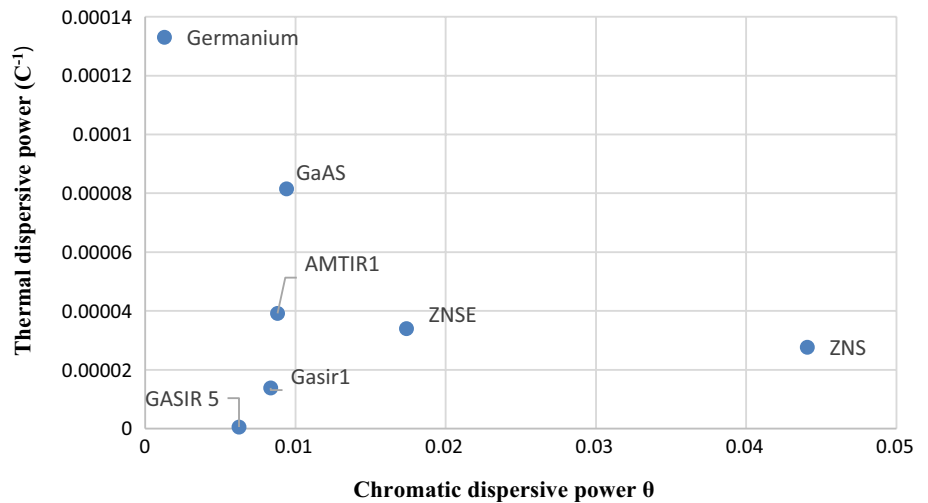
Optical design

In this work, a compact optical system with a wide field of view (12.2°) and low relative aperture (F/#1.1) is presented. Its focal length is 120 mm. The optical system consists of four lenses. The materials used were hybrid aspheric–diffractive germanium for the first lens, Gasir 5 for the second lens with a conic surface, the third lens was zinc selenide, and the fourth one was aspheric Gasir 1. As the Knoop hardness for germanium is 780 kg/mm², the first lens is of germanium to bear the harsh environment. The system has a large aperture and wide field of view, as well as it is athermalized. Also, it is achromatized for secondary spectrum “*max-color shift is 7 μ* ” and well corrected for higher-order aberrations (nearly diffraction limit performance as will be shown later) over a

Table 1 Some IR materials transparent in $\lambda = 8\text{--}12\ \mu\text{m}$ spectral band

Material	Refractive index (n)			Abbe number $V = \frac{n_m - 1}{n_s - n_i}$	dn/dT ($\times 10^{-4}$) ($^{\circ}\text{C}^{-1}$)	Thermal expansion coef- ficient $\alpha \times 10^{-6}$ ($^{\circ}\text{C}^{-1}$)	Thermal glass con- stant $\beta \times 10^{-6}$ ($^{\circ}\text{C}^{-1}$)
	$\lambda = 8\ (\mu\text{m})$	$\lambda = 10\ (\mu\text{m})$	$\lambda = 12\ (\mu\text{m})$				
Germanium	4.00669	4.00432	4.00285	783.21	4.175	5.7	133
Zinc selenide	2.41728	2.40645	2.39281	57.48	0.578	7.1	33
Zinc sulfide	2.222998	2.20025	2.17011	22.69	0.411	6.6	27
AMTIR1	2.50357	2.49749	2.49038	113.8	0.766	12	39
Gasir 1	2.49994	2.494371	2.48745	119.67	0.461	17	13
Gasir 5	2.78216	2.77706	2.77106	160.09	0.418	23.5	0.52
GaAs	3.28770	3.27807	3.26625	106.18	1.97	5	81

Fig. 1 Athermal chart for most common IR materials



temperature range extended from -40 to $+65\ ^{\circ}\text{C}$. Moreover, the system is relatively compact (140 mm). The system resolution that is compatible with an uncooled focal plane array detector (FPA) 1280×1024 has a pixel pitch $17\ \mu\text{m}$.

In this optical system, the ratio between the center thickness and diameter was considered the manufacturing process to prevent lens damage. Also, the minimum edge thickness after adding 1 mm over the clear aperture for the housing is 3 mm for the finished lens. The aspheric lens has one aspheric surface to prevent the manufacturing risk. The system is optimized for aluminum housing with thermal expansion $23 \times 10^{-6}\ \text{c}^{-1}$. Figure 2 shows the optical system layout, and Table 2 lists the optical system data. Aspheric coefficient

1st surface	4th -1.393216E-008	6th 5.090586E-014	8th -2.6295252E-016
	10th 5.9882394E-020		
8th surface	4th 3.7451177E-007	6th 9.8297086E-011	8th 7.420309994E-014

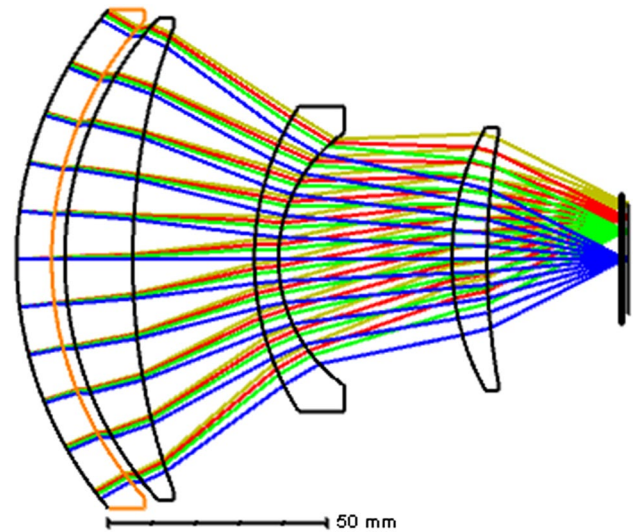
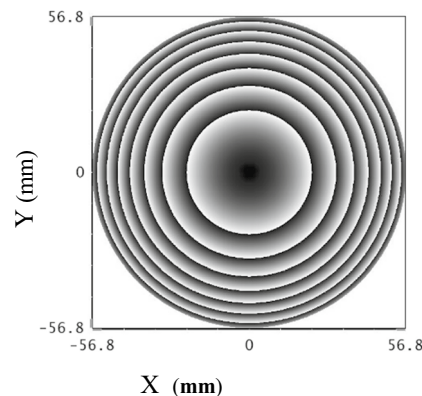


Fig. 2 Optical system layout

Fig. 3 Diffractive rings on the 1st surface X (mm)

Cycles (m)	radius (mm)
1	22.626304
2	31.454799
3	37.927806
4	43.171878
5	47.630997
6	51.535431
7	55.022871



With respect to the diffractive element, which is known as a binary element, the focal length formula is given by [4–6].

$$f = \frac{r_m^2}{2m\lambda} \tag{8}$$

where r_m is the radius of m zone.

The radii of the different steps on a binary surface (diffractive surface) that adds a phase shift by $m(2\pi)$, are shown in Fig. 3.

The main advantages of the diffractive element are the correction of the chromatic aberration and aid in athermalization, where the thermal expansion coefficient and dispersion of the diffractive element are sign opposite to that of the refractive element [5].

System evaluation

Spot diagram and encircled energy

Spot diagram and encircled energy are good ways to evaluate the optical system performance. Spot diagram is a representation of the energy distribution of a point source object at the image plane. It simulates the ray distribution at the image plane by tracing bundles of rays through the optical system. The RMS spot diameter represents about 68% of the concentrated energy [9]. The spot diagrams of the system from -40 to $+65$ °C are shown in Figs. 4a, b, and c. The maximum RMS radius of the spot diagram

at full field of view is less than $10\ \mu\text{m}$, which is less than the pixel pitch ($17\ \mu\text{m}$) over the whole temperature range. Figure 5a, b, and c shows the encircled energy graphs from -40 to $+65$ °C. More than 80% of the energy fall on $17\ \mu\text{m}$ over the temperature range. The system performance is considered nearly diffraction limit and stable over the total temperature range.

Modulation transfer function (MTF) curves

The MTF curve is an important criterion and good indication for expressing the optical system performance, especially for the image forming system. It represents the contrast modulation transfer through the optical system. It can be expressed as [10].

$$\text{MTF} = \frac{\text{image modulation}}{\text{object modulation}} \text{ modulation} = \frac{I_{\text{max}} - I_{\text{min}}}{I_{\text{max}} + I_{\text{min}}}$$

where I_{max} is the maximum intensity I_{min} is the minimum intensity

For thermal imaging system, the detector’s thermal sensitivity should be considered. As thermal sensitivity (expressed as NETD¹) increases, the threshold contrast for the target at different spatial frequencies (MRTD^{2**}) will increase. It can be expressed as:

$\text{MRTD} = \frac{\text{NETD}}{\text{MTF}}$. The NETD for uncooled detectors is quite large. So, the MTF of the optical system needs to reach the diffraction limit, at low F-number, as possible [10–12]. Figure 6a, b, and c shows that the MTF of the optical system is nearly diffraction limited and very well corrected for aberrations over the total range of temperature and full field.

Strehl ratio

Strehl ratio is one of the most meaningful ways of expressing the optical system performance. It represents the ratio

Table 2 The optical design data

Material	R1 (mm)	R2 (mm)	Thickens (mm)	Conic value
Germanium	86.838	80.192	8	
Gasir 5	81.194	163.347	15.5	2 (R2)
ZnSe	64.194	35.030	5.5	
Gasir 1	65.020	156.227	8	

¹ NETD is defined as noise equivalent temperature difference.

² MRTD is defined as minimum resolvable temperature difference.

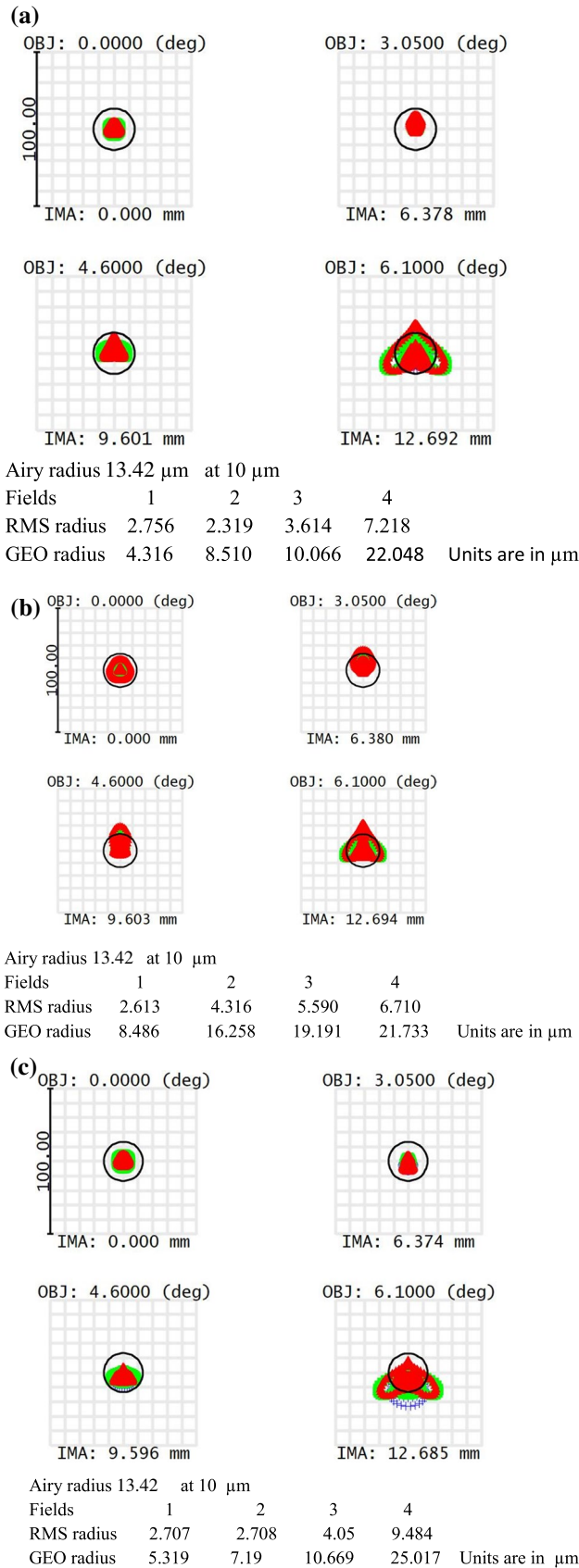


Fig. 4 **a** Spot diagram at +20 °C, **b** Spot diagram at +65 °C, **c** Spot diagram at –40 °C

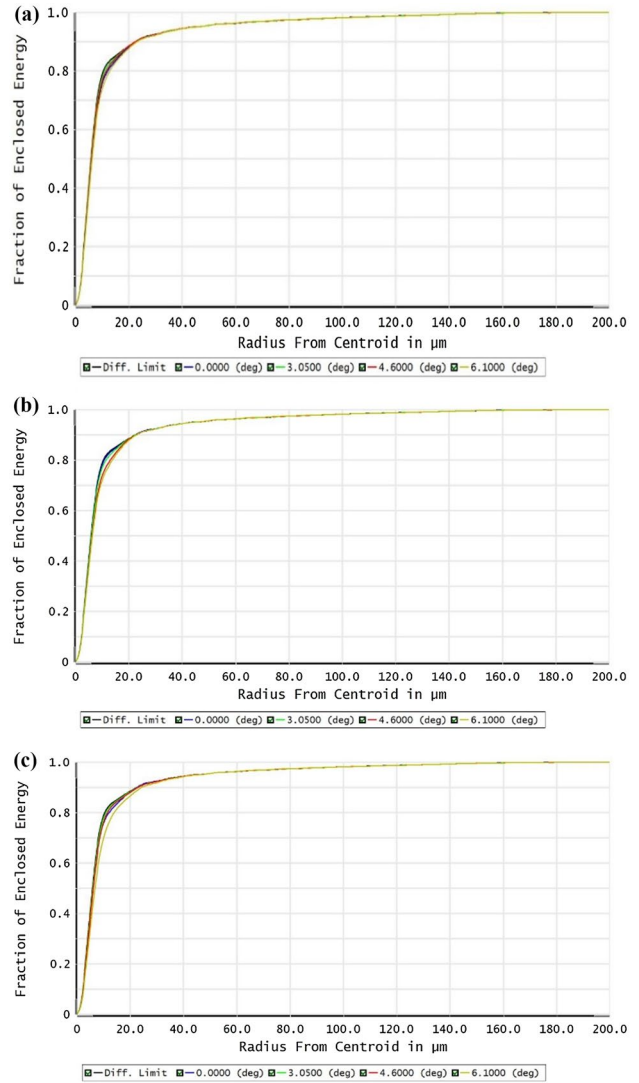


Fig. 5 **a** Encircled energy at +20 °C, **b** Encircled energy at +65 °C, **c** Encircled energy at –40 °C

between the peak diffraction intensities of an aberrated wavefront and a perfect wavefront. In this optical system, the Strehl ratio is not less than 0.95 over the whole temperature range at all field points. Figure 7a, b, and c shows the on-axis Strehl ratio over the temperature range.

In IR imaging, the system should be calibrated from the inherent emission, which is called nonuniformity correction. This can be achieved by adding a shutter between the optics and detector. Recently, several uncooled detectors are shutterless and use software techniques for this calibration.

Also, some field stops could be added to restrict the out-field stray light to reduce the incoming noise [13].

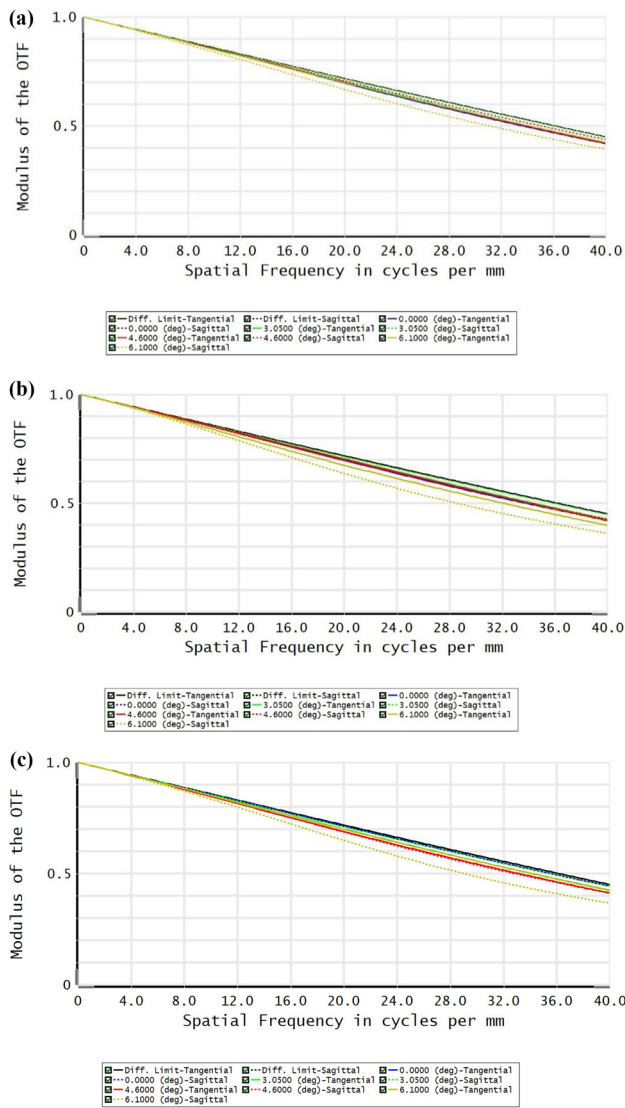


Fig. 6 **a** MTF curve at +20 °C, **b** MTF curve at -40 °C, **c** MTF curve at +65 °C

Anti-reflection coating

The refractive indices of infrared materials are high “larger than 2,” and this leads to high loss of the incident wave energy due to the high reflection. For example, the refractive index of germanium is 4 and the transmittance from one Ge lens is about 40%. For the whole system introduced in this paper, the total transmittance is only 6.6% of the incident

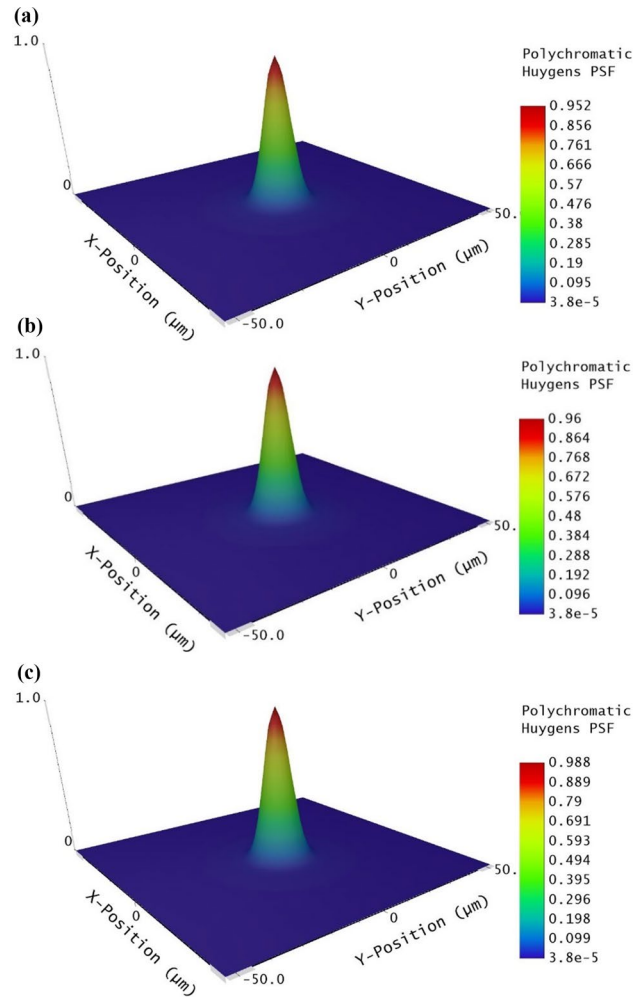


Fig. 7 **a** On-axis Strehl ratio at +20 °C, **b** On-axis Strehl ratio at -40 °C, **c** On-axis Strehl ratio at +65 °C

wave energy. To increase the transmittance of the system, the anti-reflection coating is a must. The rareness of materials transpire in IR makes the design of coating challenge. As the optical system consists of four different materials, each material has either double-layer film coating of optical thickness $t_i = \frac{\delta_i \lambda_0}{2\pi n_i}$. The condition for the double layer is a positive value [14]. The designs for four lens materials are shown in Table 3. Figure 8a, b, c, and d shows the reflectance of the lens after coating.

n_1 , n_2 , and n_s are the refractive indices of the first layer, second layer, and lens, respectively. t_i is the geometrical

Table 3 Coating configuration for optical design materials

Configuration	n_1	n_2	n_s	t_1 (μm)	t_2 (μm)	λ_0 (μm)
Air/BaF2/AgCl/ ZnSe	1.40139	1.9804	2.40644	1.46177	0.76804	10
Air/AgCl/Gasir 5/Ge	1.9804	2.77707	4.0043	1.16426	0.14235	10
Air/BaF2/ZnS / Gasir 5	1.40139	2.20025	2.77707	1.4863	0.84	10
Air/BaF2//ZnS/Gasir 1	1.40139	2.20025	2.49437	1.6951	0.98198	10

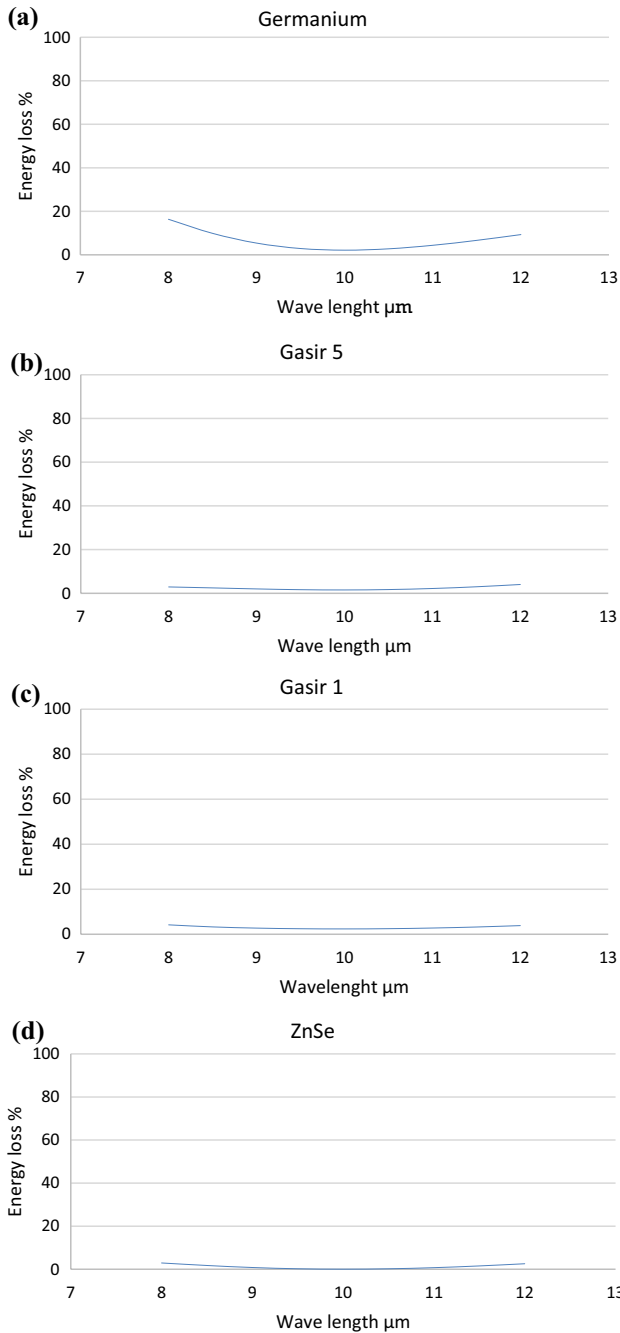


Fig. 8 **a** The energy loss of germanium lens after anti-reflection coating for 8 mm thickness, **b** The energy loss of Gasir 5 lens after anti-reflection coating for 15.5 mm thickness, **c** The energy loss of gasir lens after anti reflection coating for 8 mm thickness, **d** The energy loss of ZnSe lens after anti-reflection coating for 5.5 mm thickness

thickness of the film, and δ is the phase thickness of the film.

Also, as the materials used have high absorption coefficient (Table 4), the absorption due to materials should be taken into consideration. The transmittance of the lens after absorption loss is $T = e^{-\alpha t}$ where α is the absorption coefficient and t is the medium thickness.

By applying this coating configuration (considering the absorption loss of lenses), the transmittance of the whole system is enhanced to 75.58% at 8 μm, 94.08% at 10 μm and 81.57% at 12 μm at the center of the optical system. In spite of, the diffraction efficiency for the Kinoform surface (Binary 2) is 99.8%, but this transmittance will decrease around 1% due to the manufacturing process depending on the manufacturing tools and accuracy [15, 16].

On the front germanium lens, diamond-like carbon (DLC) protective layer could be added on the front surface to stand the harsh condition.

Conclusion

A well-corrected and optical passive athermalized optical system has been designed. The optical system is considered to work in harsh environments. The system has large aperture “109 mm,” wide field of view “12.2°,” and is relatively compact “140 mm.” With the applicable lowest number of aspheric and diffractive surfaces, the system is well corrected for higher-order aberration and nearly diffraction-limited performance. The Strehl ratio reached 0.95% at 20 °C. Also, the choosing of the optical material “using athermal chart” with the only one diffractive surface saves the system to be athermalized and achromatized for the secondary spectrum. The system performance is stable over the temperature range from – 40 °C to + 65 °C. The good MTF of the system will overcome the low sensitivity of the uncooled detector that is inversely proportional to MRTD. By applying the anti-reflection coating on the lenses, the transmittance of the system is enhanced to reach 94.04% at 10 μm at the center of the optical system. The optical system was optimized and evaluated by ZEMAX software.

Table 4 The absorption coefficient for the used material

Material	Ge	Gasir 5	ZnSe	Gasir 1	ZnS	BaF2	AgCl
Absorption coefficient (cm ⁻¹) at 10 μm	0.027	0.01	0.0005	0.05	0.2	0.00032	n/a

Acknowledgements The authors would like to express their hardly thanks to Gen\Samir Toukhy for his cooperation and advice all over this work.

Funding Open access funding provided by The Science, Technology & Innovation Funding Authority (STDF) in cooperation with The Egyptian Knowledge Bank (EKB).

Open Access This article is licensed under a Creative Commons Attribution 4.0 International License, which permits use, sharing, adaptation, distribution and reproduction in any medium or format, as long as you give appropriate credit to the original author(s) and the source, provide a link to the Creative Commons licence, and indicate if changes were made. The images or other third party material in this article are included in the article's Creative Commons licence, unless indicated otherwise in a credit line to the material. If material is not included in the article's Creative Commons licence and your intended use is not permitted by statutory regulation or exceeds the permitted use, you will need to obtain permission directly from the copyright holder. To view a copy of this licence, visit <http://creativecommons.org/licenses/by/4.0/>.

References

1. Uncooled detectors for thermal imaging cameras. FLIR technical note, Infrared Imaging News, Volume 14, Issue: 4, April 2008. http://www.flirmedia.com/MMC/CVS/AppI_Stories/AS_0015_EN.pdf
2. Cooled versus uncooled cameras for long-range surveillance. FLIR technical note
3. C. Ximin, W. XIEa, Y. BAL, X. JIA, T. XING, Athermal design for infrared refractive/diffractive/reflective hybrid optical system. *Proce. SPIE* (2014). <https://doi.org/10.1117/12.2068585>
4. D. Jianing, Z. Yinchao, C. Siying, C. He, G. Pan, Optical design and athermalization analysis of infrared dual band refractive-diffractive telephoto objective. *Proc. SPIE* **10250**, 102500H (2016). <https://doi.org/10.1117/12.2266733>
5. Y. Jiang, J. Wang, Q. Xie, W. Zhanga, E. Qua, Athermal design of refractive/diffractive hybrid infrared optical system. *Optik* **131**, 592–597 (2017). <https://doi.org/10.1016/j.ijleo.2016.11.195>
6. J. Lun, H. Yuan, D. keyan, A. Yan, W. Chao et al., Athermal design of LWIR hybrid refractive/diffractive optical system. *Proc. SPIE* **9618**, 96180Y (2015). <https://doi.org/10.1117/12.2193320>
7. M. Bass, *Hand book of optics* (McGraw-Hill, New York, 1995)
8. Y. Tamagawa, S. Wakabayashi, T. Tajime, T. Hashimoto, Multilens system design with an athermal chart. *Appl. Opt.* **33**, 8009 (1994). <https://doi.org/10.1364/AO.33.008009>
9. Zemax OpticStudio 18.4 “User manual”, Zemax, 2021
10. R.E. Fischer, *Optical system design* (SPIE press McGraw-Hill, Bellingham, 2008)
11. A. Daniels, *Field guide to infrared systems* (Detectors, Bellingham, 2010)
12. Thomas Willams (2009) Thermal imaging camera. CRC press by Taylor and Francis group
13. E.C. Fest, *Stray light analysis and control* (SPIE Press, Bellingham, 2013)
14. M. Mohamed, E.-Z. El-Sayed, F. Samy, Y. Gamal, A. Reda, Enhancing silicon solar cell efficiency with double layer anti-reflection coating. *Turk. J. Phys.* (2016). <https://doi.org/10.3906/z-1508-14>
15. V. Moreno, J.F. Román, J.R. Salgueiro, High efficiency diffractive lenses: deduction of kinoform profile. *Am. J. Phys.* **65**(6), 556–562 (1997)
16. Nam-Hyong Kim, (2021) How to model diffractive optics using the binary 2 surface. ZEMAX knowledgebase

Publisher's Note Springer Nature remains neutral with regard to jurisdictional claims in published maps and institutional affiliations.